Article

Dating the Sedimentary Protolith of the Daldyn Group Quartzite, Anabar Shield, Russia: New Detrital Zircon Constraints

Nikolay I. Gusev [1,*], Lyudmila Yu. Sergeeva [1] and Sergey G. Skublov [2,3]

[1] Karpinsky Russian Geological Research Istitute of Geology (VSEGEI), 199106 St. Petersburg, Russia; sergeeva.luda02@yandex.ru

[2] Institute of Precambrian Geology and Geochronology, Russia Academy of Sciences (IPGG RAS), 199034 St. Petersburg, Russia; skublov@yandex.ru

[3] Saint-Petersburg Mining University (Mining University), 199106 St. Petersburg, Russia

* Correspondence: Nikolay_Gusev@vsegei.ru; Tel.: +7-81232-89-124

check for updates

Abstract: Quartzites and paragneisses of the Archean granulite series of the Anabar Shield (Siberian Craton, Russia) are described geochemically. The Sm-Nd isotope systematics of the rocks and the U-Pb age (SHRIMP II) and geochemistry of zircons from quartzites and paragneisses are studied. Newly formed zircons from quartzites display geochemical characteristics of the magmatic type and were produced by rock anatexis upon granulite-facies metamorphism. The Paleoproterozoic age of the latest detrital zircons, 2250 ± 24 Ma, constrains the maximum age of sedimentary rock deposition. The anatectic rims around detrital zircons were formed ca. 2000 ± 9 Ma ago. The time of deposition of the sedimentary protolith of gneisses and quartzites falls within the age interval of the above-mentioned dates and is tentatively accepted as 2.1 Ga. The presence of Paleoproterozoic metasedimentary rocks in the Daldyn Group implies the tectonic heterogeneity of the series and the existence of Paleoproterozoic rock bodies among the predominant Archean rock sequences.

Keywords: Anabar Shield; granulites; Archean; Paleoproterozoic; quartzites; zircon; geochemistry; U-Pb age; Sm-Nd systematics

1. Introduction

Siberian Craton is the largest Precambrian continent in the north of Asia. The basement of the Siberian Craton represents a Paleoproterozoic collage of Precambrian highly metamorphosed terranes [1–3], which is overlain by Mesoproterozoic to Lower Cretaceous sedimentary rocks and Mesozoic flood-basalts (traps). The current understanding of the age and structure of the Siberian cratonic basement has been outlined mostly through studies of exposed rocks in the Anabar and Aldan shields and the Olenek, Kan, Birusa, and Sharyzhalgai uplifts (Figure 1).

According to a number of studies, the Siberian craton is composed of several Archean and Early Proterozoic superterranes (Tungus, Anabar, Aldan, Stanovoy) that are believed to have assembled into a single structure and finally stabilized at 1.8–2.1 Ga. Superterranes are suggested to have an ancient granulite-gneiss or granite-greenstone basement. The assembling event is marked by a widespread collision-related granulite metamorphism and collisional and post-collisional granitic magmatism [1]. The Siberian Craton is also divided into several tectonic provinces (Figure 1: Tungus, Anabar, Olenek, Aldan) consisting of heterogeneous terranes [1]. The Anabar Shield is an exposed block of the basement of the Anabar province.
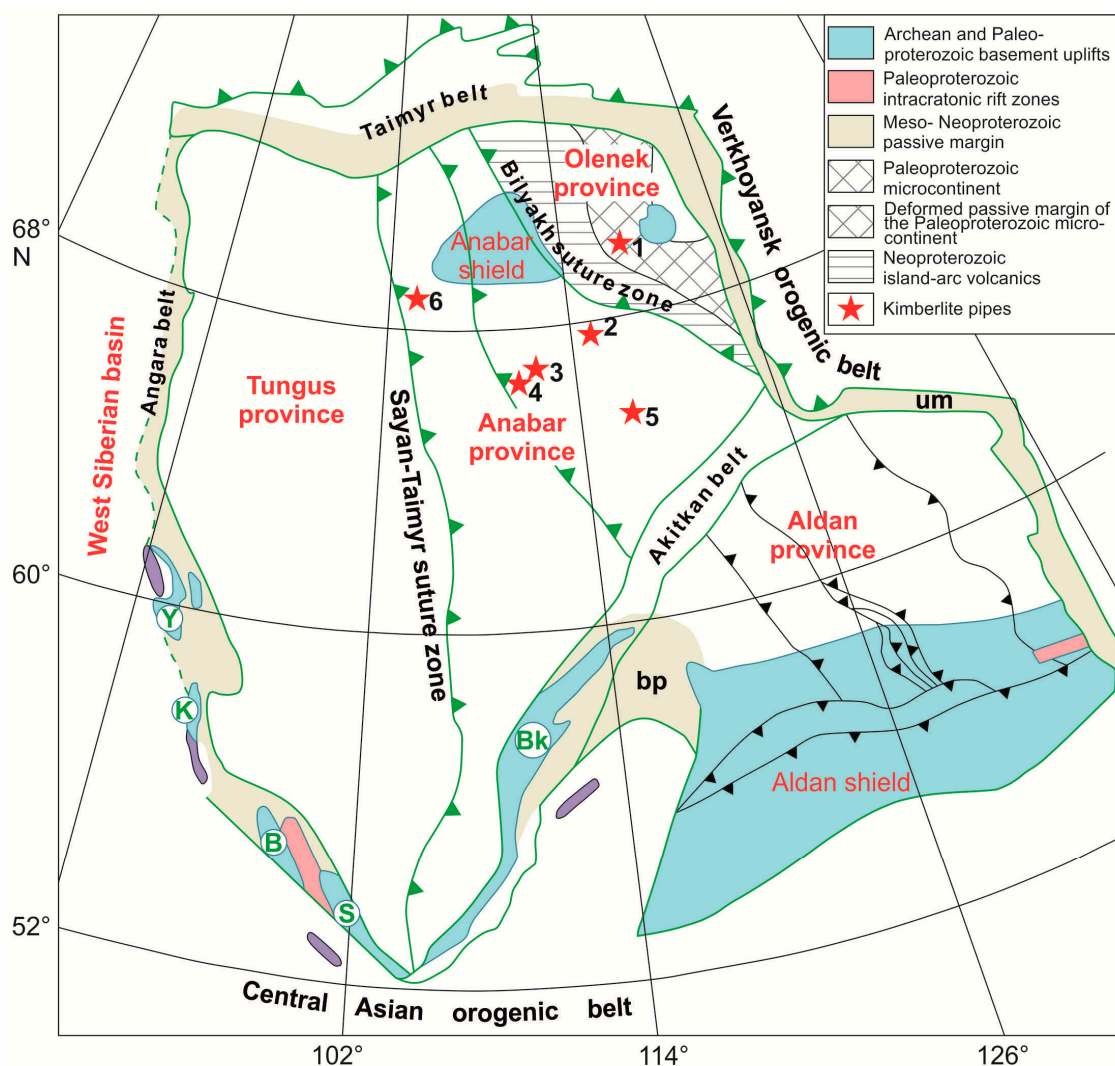
Figure 1. Geological scheme of the Siberian craton (modified after [1–3]. Green lines delineate the boundaries of the Siberian craton and its major units. Red stars represent kimberlite fields: 1—Kuoyka field; 2—Muna field; 3—Daldyn field; 4—Alakit field; 5—Nakyn field; 6—Kharamai field. Paleoproterozoic intracratonic rift zones: ub-Ulakano-Billikean, ui-Urik-Iya. Archean-Paleoproterozoic basement uplifts: B—Birusa block; Bk—Baikal uplift; K—Kann uplift; S—uplift; Y—Yenisey uplift. Riphean sedimentary succession areas: bp—Baikal-Patom; um—Uchur-Maya.

The Anabar shield (Figure 2) is composed mainly of rocks metamorphosed in the granulite facies, which are combined into the Archean Daldyn and Upper Anabar groups and the Paleoproterozoic Khapchan Group [1,4]. The Daldyn and Upper Anabar groups consist mostly of hypersthene plagiogneisses and subordinate amounts of orthopyroxene-clinopyroxene-plagioclase schists (metabasites), with quartzite beds and, locally, beds of aluminous schists and silicate marble. The Khapchan Group is made up of metasedimentary garnet gneisses, beds of metacarbonate rocks, and rare horizons of hypersthene plagiogneisses. The Early Proterozoic shear zones comprise reworked Archean granulites (including anorthosites, tectonites, and granite-migmatites) metamorphosed to the amphibolite facies [5]. Numerous U-Pb zircon dates and data on the Sm-Nd isotopic systems [1,4–8] show that the dominant rocks of the Daldyn and Upper Anabar groups are granulites, whose protoliths have an age of 3.0–2.8 Ga. Metamorphosed anatectic granitoids with an age of 3.34 Ga are less common [7,8]. Sometimes mafic xenoliths containing Eoarchean zircon are found in them [8].
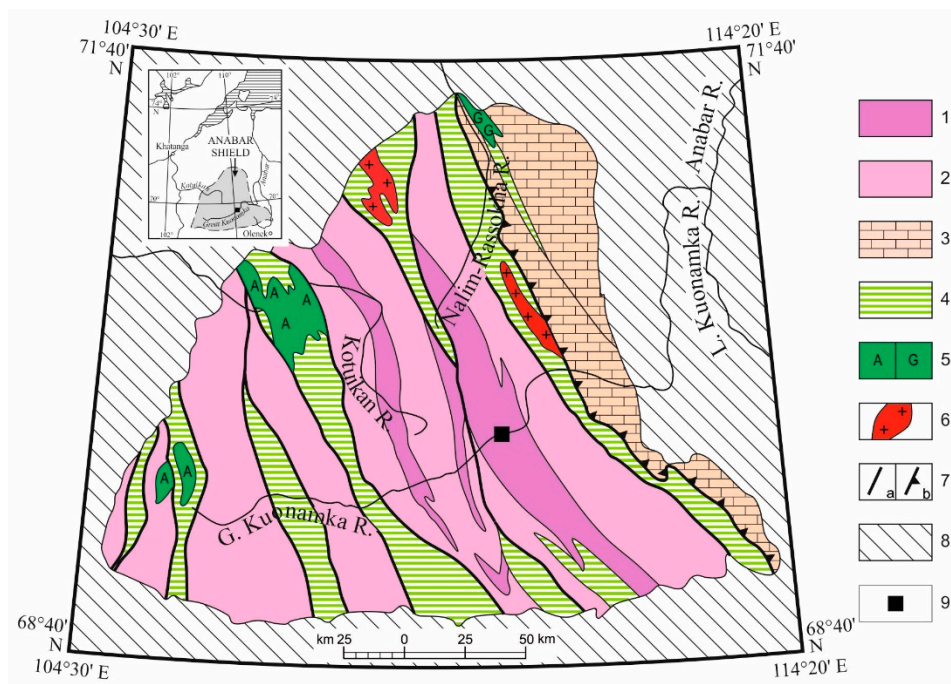
Figure 2. Schematic geological map of the Anabar Shield. (1–3) Archean and Early Proterozoic metamorphic rocks: (1) Daldyn Group; (2) Upper Anabar Group; (3) Khapchan Group; (4) Early Proterozoic shear zones. (5) Intrusive rocks: (A) anorthosite and (G) gabbroids. (6) autochthonous and parautochthonous granitoids. (7) Major faults: (a) steep faults and (b) overthrusts. (8) platform cover; (9) area of Figure 2.

The oldest Daldyn Group comprises the Bekelekh and Kilegir sequences, which contain various quantities of crystalline schist and gneisses. The Bekelekh sequence is dominated by meso and melanocratic two-pyroxene and hypersthene plagiogneisses. The Kilegir sequence displays a more diverse petrographic composition; it contains such characteristic rocks as quartzite (up to 5%), which forms lenses and beds stretching for several kilometers. The quartzites exhibit signs of sedimentary origin and are used as indicators for distinguishing between the Kilegir and Bekelekh sequences.

The detrital zircons are studied in the quartzites, and their U-Pb age is estimated to constrain the maximum sedimentation age of original parental rocks and obtain evidence for the source area to describe the tectonomagmatic evolution and conduct paleogeographic reconstructions and correlations [9–13].

Detrital zircons in three quartzite samples from the Anabar Shield showing the oldest (Paleo and Eoarchean Nd-model age of the protolith [7,14]) were dated to estimate the time of formation of the Siberian Craton's continental crust. The oldest detrital zircons from quartzites in the upper reaches of the Nalim-Rassokha River yield an age of 3570 Ma, but the sedimentary protolith of Daldyn quartzites is not older than 3254 ± 38 Ma [8]. Two Daldyn quartzite samples from the Khataryk River mouth (Figure 3, samples 820 and 832-1) are dominated by detrital zircons dated at 3487 ± 21 Ma [15], but the depositional age of the sedimentary protolith of quartzites is unknown.

The analysis of zircons from quartzites metamorphosed under granulite facies conditions is complicated by the polygenetic structure of grains, the latter consisting of detrital zircon cores reworked to a different extent via granulite facies metamorphism and metamorphic shells. Some of the zircon grains analyzed possess several metamorphic shells, which indicate multiple metamorphisms. Typically, the metamorphic shells of the Anabar Shield granulites result from the latest Paleoproterozoic metamorphism [4,5]. The aim of the present study is to date the sedimentary protolith of quartzites in Daldyn granulites at the Khataryk River mouth and in the transition zone between the Bekelekh and Kilegir sequences.
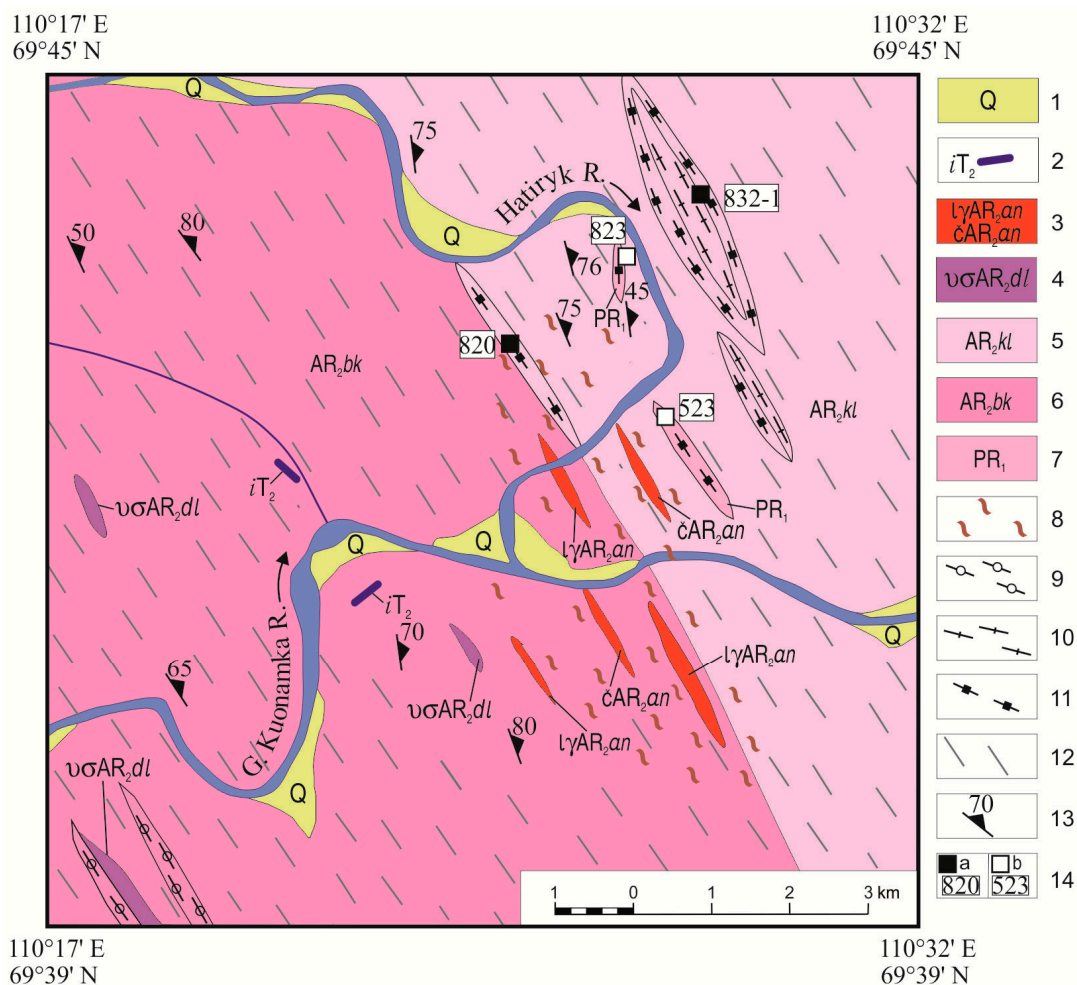
Figure 3. Geological map of the estuary part of the Khataryk River. (1) Quaternary rocks; (2) kimberlites; (3) charnockites, enderbites, and alaskan granites; (4) metamorphosed peridotites and pyroxenites. (5,6) Daldyn Group: (5) Kilegir sequence, including two-pyroxene schists, plagiogneisses, and quartzites; (6) Bekelekh sequence, including hypersthene, two-pyroxene plagiogneisses, and schists. (7) Paleoproterozoic metasedimentary rocks; (8) migmatization; (9) clinopyroxene and scapolite-clinopyroxene plagiogneisses; (10) garnet and pyroxene plagiogneisses; (11) quartzites; (12) orthopyroxene, two-pyroxene, and hornblende-pyroxene plagiogneisses; (13) strike and dip of gneissosity and foliation. (14) Localities and numbers of samples: (a) quartzites previously studied [9]; (b) presented in this paper.

2. Materials and Methods

The concentrations of the major and trace elements in rocks were determined by XRF («Thermo Fisher Scientific (Ecublens) SARL», Ecublens, Switzerland) and ICP-MS (PerkinElmer Life and Analytical Sciences, Inc., Waltham, MA, USA) at a laboratory of the Karpinsky Institute. The analytical uncertainties of the XRF analysis were no greater than 5 relative %. The detection limits of the trace elements were 0.005 to 0.1 ppm, and the analyses were accurate to 2–7 relative % on average.

The U-Pb dating of zircons was conducted on a SHRIMP-II probe at the Center of Isotopic Research of the Karpinsky Institute following conventional methods [16]. Areas (spots) for dating were selected using optical (in transmitted and reflected light) and cathodoluminescence (CL) images that showed the inner structure and zoning of the zircons. The intensity of the primary molecular oxygen beam was 4 nA, the diameter of the spot (crater) was 25 μm, and its depth was 2 μm. The raw data were processed with the SQUID software (Berkeley Geochronology Center, Berkeley, CA, USA) [17]. The $^{206}Pb/^{238}U$

ratios were normalized to 0.0668, a value for the TEMORA zircon standard dated at 416.75 Ma [18]. The uncertainties of individual analyses (ratios and ages) are reported at a 1σ level, the uncertainties of the calculated values of concordant ages and intercepts with a concordia are presented at a 2 σ. level. The plots were constructed using the ISOPLOT/ET program (Berkeley Geochronology Center, Berkeley, CA, USA) [19].

The zircons were analyzed for trace elements by secondary ion mass spectrometry (SIMS) on a Cameca IMS-4f probe at the Yaroslavl Branch of the Physical—Technical Institute, Russian Academy of Sciences; the procedure is described in [20]. The analysis was conducted accurate to better than 10% for elements whose concentrations were higher than 0.1 ppm and 30–50% at concentrations lower than 0.1 ppm. The zircon crystallization temperature was determined by the Ti-in-Zrn thermometer [21].

The Sm–Nd isotope composition was studied using conventional procedures for the separation of elements. The isotope measurements were conducted on a TRITON TI mass spectrometer (ThermoQuest Finnigan MAT, Bremen, Germany) at the Center of Isotopic Research at the Karpinsky Institute. Calculation according to the formula $\varepsilon_{Nd}(T) = [(^{143}Nd/^{144}Nd_{SAMPLE,t}/^{143}Nd/^{144}Nd_{CHUR,t}) - 1] \times 10^4$ is performed using the following values of isotope ratios for the chondritic uniform reservoir (CHUR): $^{147}Sm/^{144}Nd = 0.1967$ and $^{143}Nd/^{144}Nd = 0.512638$ [22]. The single-stage model age $T_{Nd}(DM)$ is defined as follows:

$$T_{Nd}(DM) = \frac{1}{\lambda} ln\left[\frac{\left(^{143}Nd/^{144}Nd\right)_{sample,today} - \left(^{143}Nd/^{144}Nd\right)_{DM,today}}{\left(^{147}Sm/^{144}Nd\right)_{sample,today} - \left(^{147}Sm/^{144}Nd\right)_{DM,today}} + 1\right]$$

The $T_{Nd}(DM)$ was calculated relative to the depleted mantle, with $^{147}Sm/^{144}Nd = 0.2136$ and $^{143}Nd/^{144}Nd = 0.51315$ [23].

The studied rocks have a sedimentary protolith; therefore, to determine the age of the rocks in the denudation area, a two-stage model age $T_{Nd}(DM-2st)$ was calculated. The two-stage model age ($T_{Nd}(DM-2st)$) can be obtained from the single stage ($T_{Nd}(DM)$) model age by the equation [23]:

$$T_{Nd}(DM - 2st) = T_{Nd}(DM) - (T_{Nd}(DM)\ T_{STRAT})\left[\frac{f_{CC} - f_{sample}}{f_{CC} - f_{DM}}\right]$$

where T_{STRAT} is the sample evolution from the time of deposition; $f_{CC} = -0.4$, $f_{DM} = 0.08592$ is the $f_{Sm/Nd}$ value of the DM reservoir.

Mineral symbols are according to [24].

3. Sample Descriptions

Rocks in the transition zone between the oldest Bekelekh sequence (AR_2bk) and the younger Kilegir sequence (AR_2kl) were studied. In the coarse-grained Grt-Cpx gneiss exposure (Figures 3 and 4, outcrop 823), milky-white quartzites, occurring as 5–10 cm thick intercalations, alternate with clinopyroxene gneisses enriched in coarse garnet aggregates (Figure 4). On the hanging wall, they are in contact with schist (Figure 4, sample 823-2) which passes upwards into migmatized orthopyroxene gneisses.
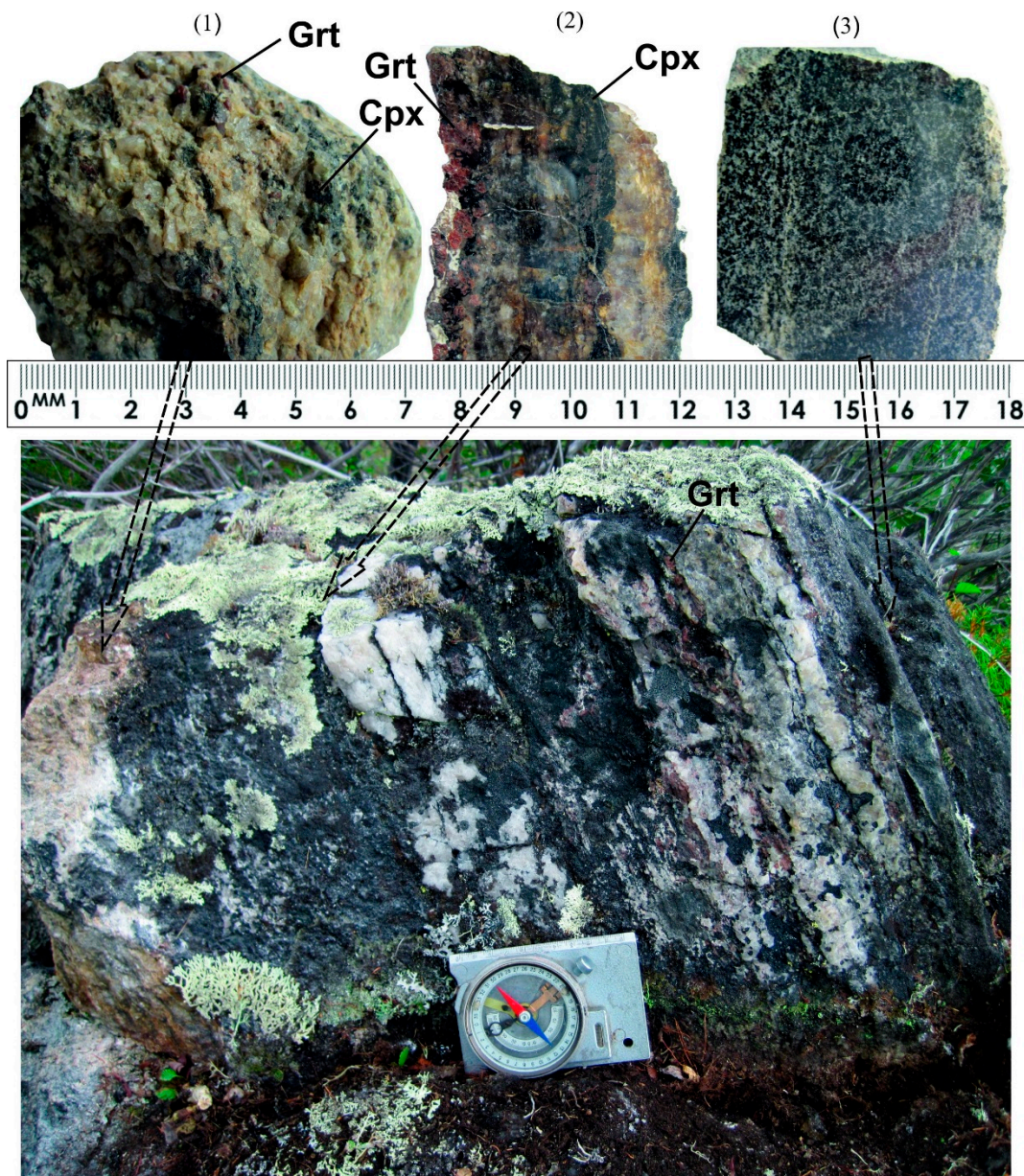
Figure 4. Outcrop 823. 1—coarse-grained Grt-Cpx gneisses (sample 823); 2—the contact of Grt-Cpx gneisses with quartzites; 3—Cpx-Opx schists (sample 823-2). Coordinates: 69°43′20″N, 110°29′33″E.

4. Petrography

Coarse-grained Grt-Cpx gneisses (sample 823) contain Qtz (50–53%, The content is given in volume%), Pl (An36) (20%), Cpx (18%), Grt (5–7%), Bt (2%), and Mag (2%). The rock is thick-banded in the thin section. Its melanocratic portion contains clinopyroxene-plagioclase aggregates, with relatively equal Cpx and Pl concentrations. Garnet aggregates with abundant Qtz, Pl, and Cpx inclusions are confined to silicification bands composed of coarse isometric quartz grains. The late crystallization stage is characterized by coarse grained biotite and garnet. The quartzite of sample 823-1 consists of Qtz (68–70%), Cpx (15%), Grt (7–10%), Bt (3%), and Mag (2%). The other quartzite (sample 523) consists of Qtz (80%), Mi (10%), Pl (An7) (8%), and Bt (1%). The quartzite of sample 820 consists of Qtz (90%), Sill (4%), Mi (4%), Bt (1%), and Ilm (1%). The quartzite of sample 831-1 consists of quartz (98%), Sill (1%), and Bt (1%). The two-pyroxene schists (sample 823-2) consist of Pl (An70) (40%), Cpx (7%), Opx (35%), and Mag (6%). Single large apatite grains are found sporadically; superimposed

minerals are presented by Qtz (10%) and Bt (2%). The boundary with quartzite in thin section is sharp, but coarse elongated quartz grains contain crystalline schist inclusions and garnet grains elongated concordantly with quartz grains.

5. Geochemical Data

Coarse-grained Grt-Cpx gneisses (sample 823) were identified as para-rocks based on the following ratios: MgO/CaO = 2; P_2O_5/TiO_2 = 0.03 [25]. Elevated Cr (114 ppm), Y (157 ppm), Zr (541 ppm), and Nb (7.92 ppm) concentrations may be ascribed to the enrichment of chromite, zircon, and monazite detritus in sedimentary rocks (Table S1). The spider diagram of sample 823 shown on Figure 5 indicates a positive U anomaly and a negative P anomaly. The rare earth elements (REE) distribution (ΣREE = 141 ppm) displays the predominance of heavy rare earth elements (HREE) over light rare earth elements (LREE), which is possibly associated with garnet detritus and the growth of metasomatic garnet; the Eu-minimum (Eu/Eu* = 0.56) is well-defined. The garnet quartzite from sample 823-1 contains less REE (ΣREE = 30.16 ppm) and displays a distribution pattern similar to that of coarse-grained gneiss. The spider diagram in Figure 5a shows positive Ba and Zr anomalies and negative Sr and Ti anomalies.
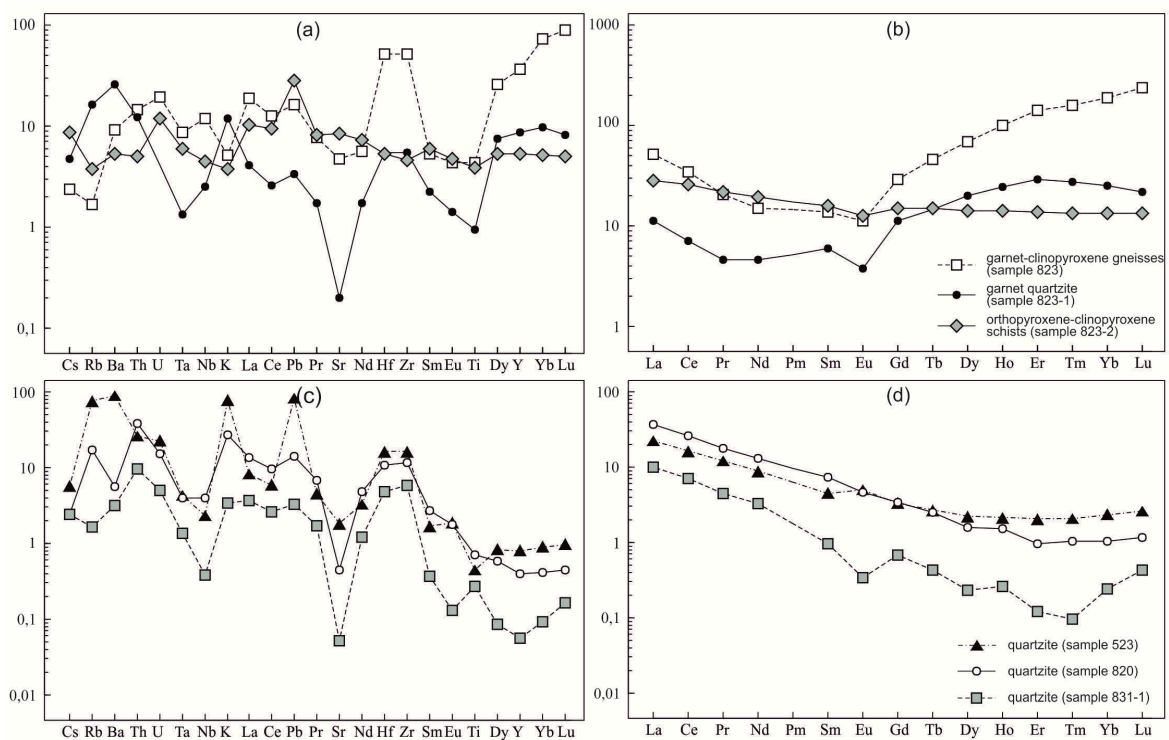

Figure 5. (**a**,**c**) Primitive mantle-normalized abundances of trace elements; [26] (**b**,**d**) chondrite-normalized [26] REE patterns for zircons.

The quartzites (samples 523, 820, 831-1) generally display low values (Al_2O_3/SiO_2) (0.01–0.05) and are consistent with the values (Na_2O/Al_2O_3) (0.01–0.20) in terrigenous rocks [27]. The values ($Fe_2O_3+FeO+MnO/Al_2O_3+TiO_2$) (0.05–0.14) indicate the aluminous composition of pelites. The chemical alteration index value, ($Al_2O_3/(Al_2O_3+CaO+Na_2O+K_2O)$), varies considerably (43–90), indirectly indicating a difference in source areas.

The total REE concentration in the quartzite is in the range of 24–36 ppm (except for sample 831-1—9 ppm). The REE distribution displays a differentiated pattern (La_N/Yb_N = 9–39). The quartzites from samples 820 and 523 show Eu/Eu* = 0.93–1.29, while sample 831-1 exhibits the most negative

Eu anomaly (Eu/Eu* = 0.42). The rocks contain low Th (0.76–3.03 ppm) and U (0.10–0.46 ppm) concentrations; the Th/U ratio is 4.52–9.77.

Orthopyroxene-clinopyroxene schists (sample 831-2) contain elevated Cr (177 ppm) and Ni (126 ppm) concentrations (Table S1); the spider diagram in Figure 5 shows positive U and Pb anomalies. The REE concentration is low (ΣREE = 49.94 ppm) and the distribution shows a flat pattern $(La/Yb)_N$ = 1.98 with a slight minimum Eu anomaly (Eu/Eu* = 0.82).

6. U-Pb Data

Age dating was performed for zircons from coarse-grained Grt-Cpx gneisses (sample 823), garnet quartzite (sample 823-1), and quartzite (sample 523) (Table S2). In outcrop 823, a similar zircon monofraction from coarse-grained Grt-Cpx gneisses and garnet quartzite consists of yellow transparent and semi-transparent prismatic and rounded idiomorphic and sub-idiomorphic crystals and fragments. The crystals are 200–400 μm long, with a coefficient of elongation (K_y) of 1–2. The zircon grains are polygenetic in CL image; three zircon generations were identified (Figure 6). The cores dominantly display poor luminescence, sometimes (grain, point with analysis 8.1) with fine rhythmic zoning. Some of the cores are surrounded by thin brightly luminescent rims (analytical points 9.2 and 7.2) varying in width, partly dissolved upon being overgrown by rims, which shows grey luminescence. The grey rims are much thicker; such grey luminescent zircons make up individual coarse grains with coarse concentric zoning and the sectorial structure of the central portions of crystals. Grey zircons from gneisses display a concentric structure and finer rhythmic zoning around the black cores. The internal rhythmic zones and lighter external rims of the gneisses were dated separately. The neoformation of zircon in the quartzites is well-defined, but detrital zircons in the cores are much worse preserved. The radial fracturing in the back-scattered electron (BSE) image is conspicuous. Fractures begin to form at the boundary of cores that are dark in CL and spread into zircon grain, which is grey in CL, towards the grain margins. The fracturing was caused by a differentiated and more intense zircon metamictization and by the increasing volume in the U- and Th-enriched cores, and was followed by the alteration of low U- and Th rims [28].

The cores and rims of 14 zircon grains from Grt-Cpx gneisses were analyzed. The cores are mainly black in CL, but they sometimes contain zircon fragments with well-defined rhythmic zoning (grains with analyses 1.1, 4.1, 5.1, 6.1, 7.1), in which Th/U = 0.13–0.91.

The maximum $^{207}Pb/^{206}Pb$ age value in the core from the analysis 6.1 is 2723 ± 9 Ma, but it is highly discordant (D = 8%). The age of 2364–2250 Ma was obtained for three cores; it should be noted that analysis 4.1 yielded an age of 2316 ± 19 Ma with a low discordance (D = 1%). The black homogeneous cores dated (2107–2048 Ma) display low Th/U ratios of 0.04–0.10, typical of metamorphic zircons.

The zircon cores in garnet quartzite from sample 823-1 show the age range $^{207}Pb/^{206}Pb$ of 2758–2566 Ma; the smaller value of 2214 ± 11 Ma, at a point with analysis 3.1, is due to the trapping of the surrounding grey zircon by the analytical crater (Figure 7). The oldest value of 2758 ± 11 Ma (D = −3%) was obtained for a zircon core with analysis 8.1 with a well-defined rhythmic zoning. In the REE distribution diagram (Figure 7), it is characterized by the composition of magmatic zircons and by the lowest Ti-in-Zrn temperature (T_{Ti}^{Zir}) of 760 °C. Other zircon cores are enriched in LREE and are shifted towards hydrothermal zircons with respect to the trace element composition (Figure 8a). The cores display a Th/U ratio of 0.38 and mean U concentrations of (102 ppm); Th (256 ppm); Y (1404 ppm); Hf (7446 ppm); ΣREE 976 (ppm) (Table S3). The temperature reaches a maximum value of 858 °C for the most enriched REE zircon with 5.1 analysis.
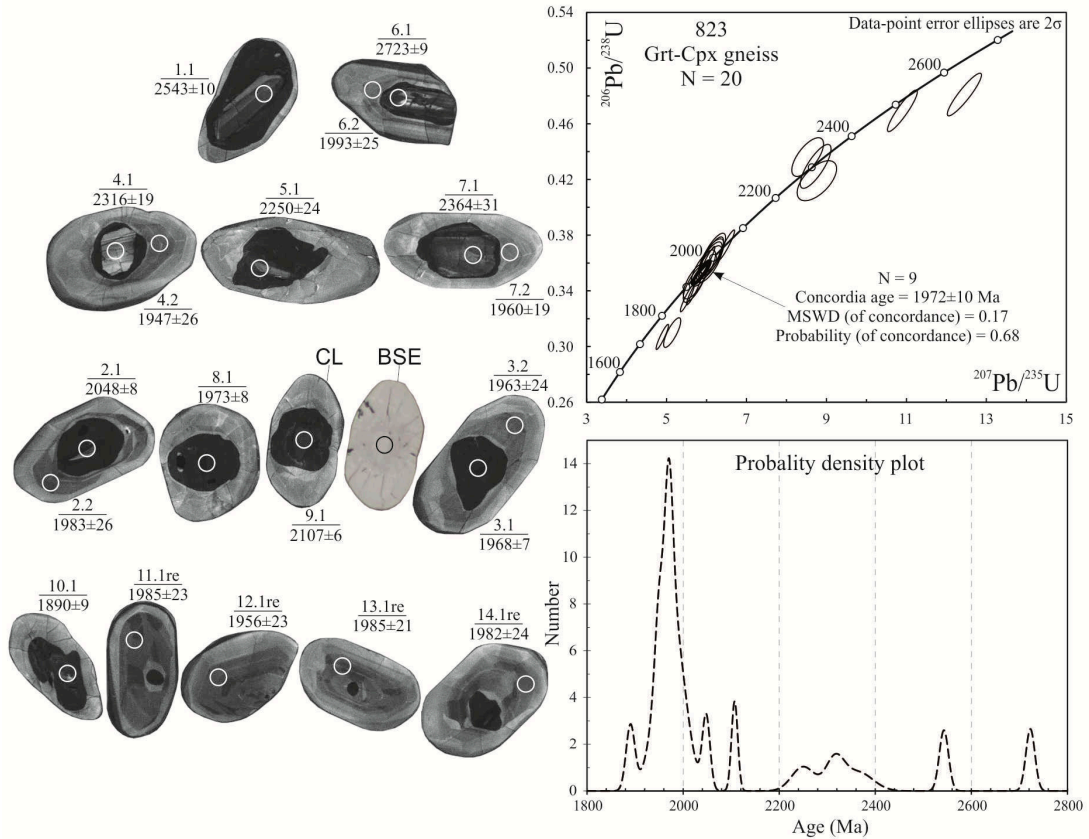
Figure 6. Cathodoluminescence (CL) images and ages of zircons from the garnet–clinopyroxene gneiss (sample 823). White circles mark analytical craters, and the nearby numerals are the numbers of the analytical spots (numerators) and ^{207}Pb/^{206}Pb age (denominators). The craters are 20 μm in diameter.

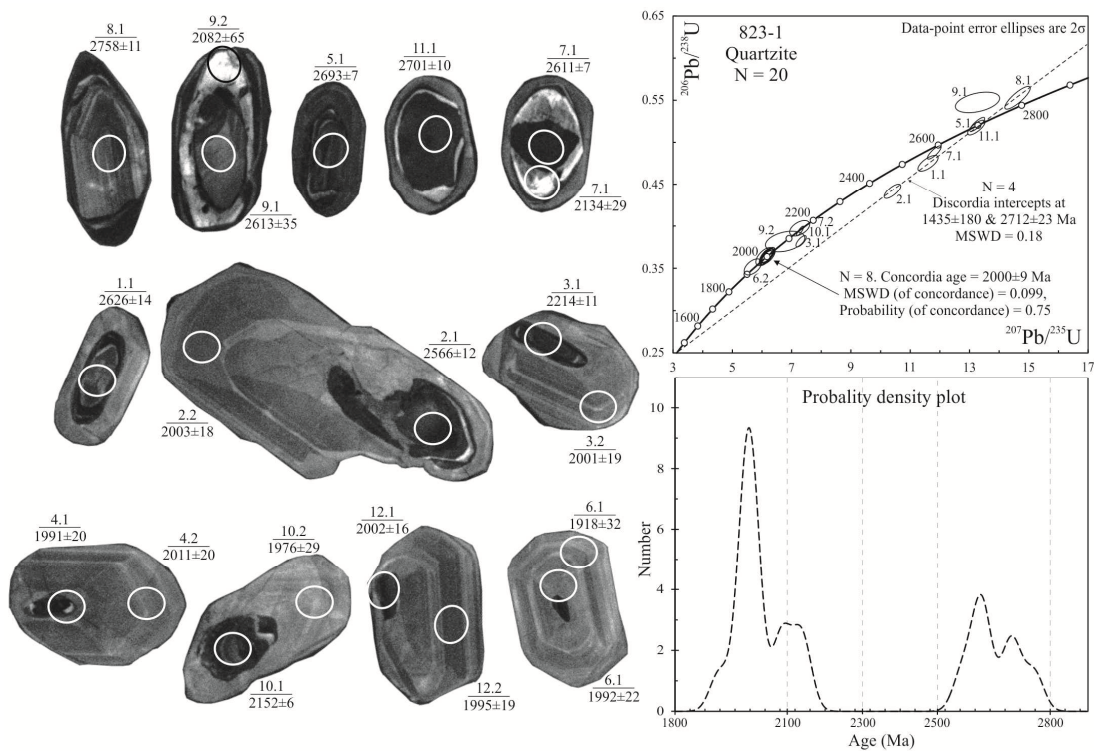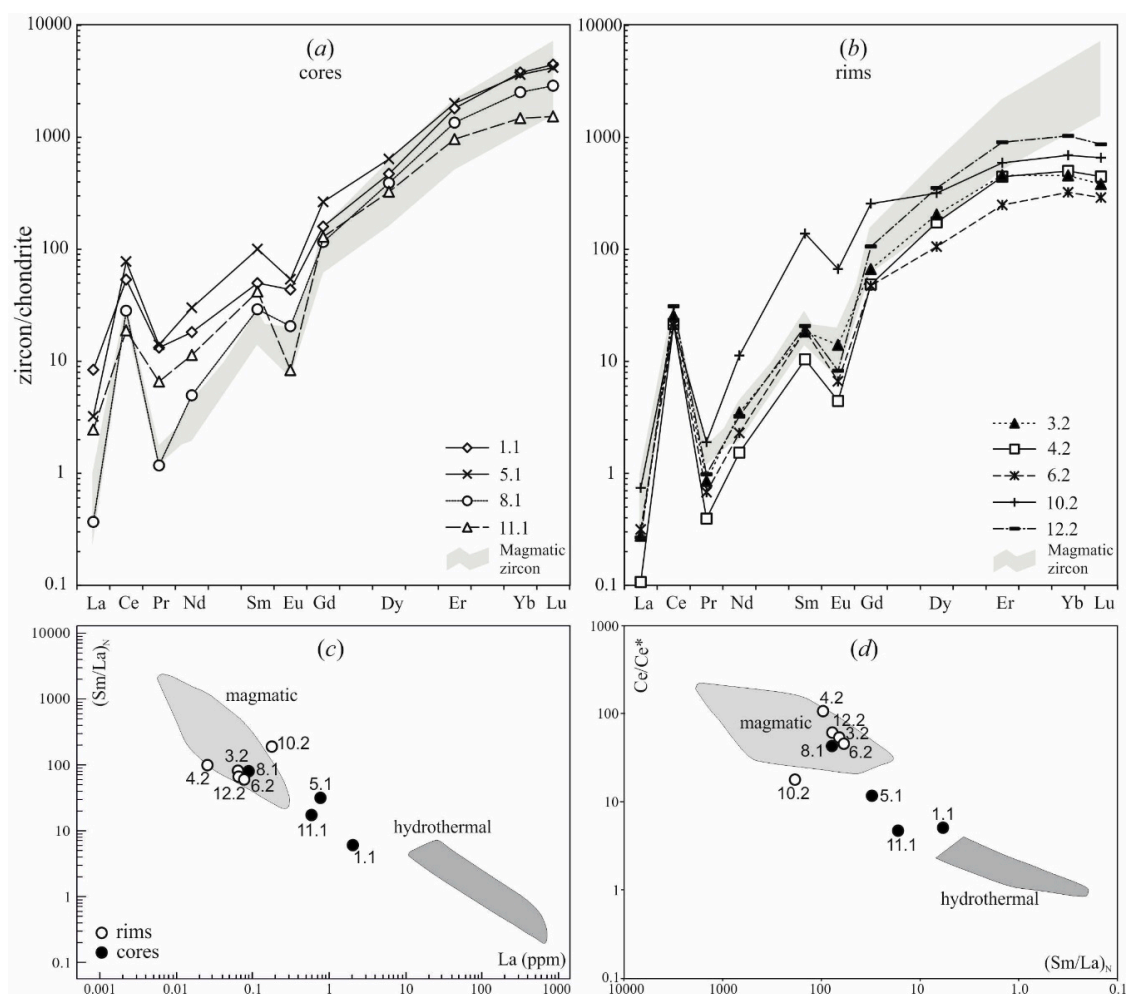**Figure 7.** CL images and age of zircons from the garnet quartzite, sample 823-1.

Figure 8. (**a**,**b**)—Chondrite-normalized REE patterns of zircon from the garnet quartzite, sample 823-1. Pattern numbers correspond to the numbers of analytical spots in Figure 6. The grey field corresponds to the composition of magmatic zircon according to [29]. (**c**,**d**)—Diagrams for distinguishing magmatic zircon from the hydrothermal one according to [29].

The grey rims and the individual grains of CL-grey zircon show a REE distribution pattern and indicator ratios $(Sm/La)_N$ and Ce/Ce* which are consistent with those of magmatic zircons (Figure 8b). In contrast to the cores, the grey zircon of the rims contains low concentrations (mean values in ppm)—U 89, Th 86, Y 616, ΣREE 296—but displays a higher Th/U ratio of 1.0 and Hf concentration of 9278–10,182 ppm. Grey zircons, in contrast to typical magmatic zircons, are poor in HREE (flattening of the spectra from Er to Lu) and display a low $(Lu/Gd)_N$ ratio of 2.6–9.2, which indicates zircon growth in the presence of garnet (Gd-concentrating mineral), i.e., under granulite-facies conditions of metamorphism. A quite sustained value = 781–793 °C is noted. The age of 2000 ± 9 Ma with a high concordance (probability of concordance = 0.75) was obtained from eight analyses. It is understood as the crystallization time of grey zircon grains and rims.

The zircons from quartzite in sample 523 are brown-colored, and their sub-idiomorphic oval grains are transparent to semi-transparent and fractured (Figure 9). The grains are 100–200 µm long with a K_y of 1–2.5. The zircons dominantly display a poor luminescence in CL, a black color prevails, there is no luminescence, and the metamorphic rims are either thin or poorly-defined. Zoning in crystals is mainly observed as a combination of fine and coarse banding with signs of sectorial zoning (point 12.1). Zoning is mainly truncated by the grain margins; zoning subparallel to grain margins is less common (6.1, 12.1, 13.1–2326 Ma, 19.1).
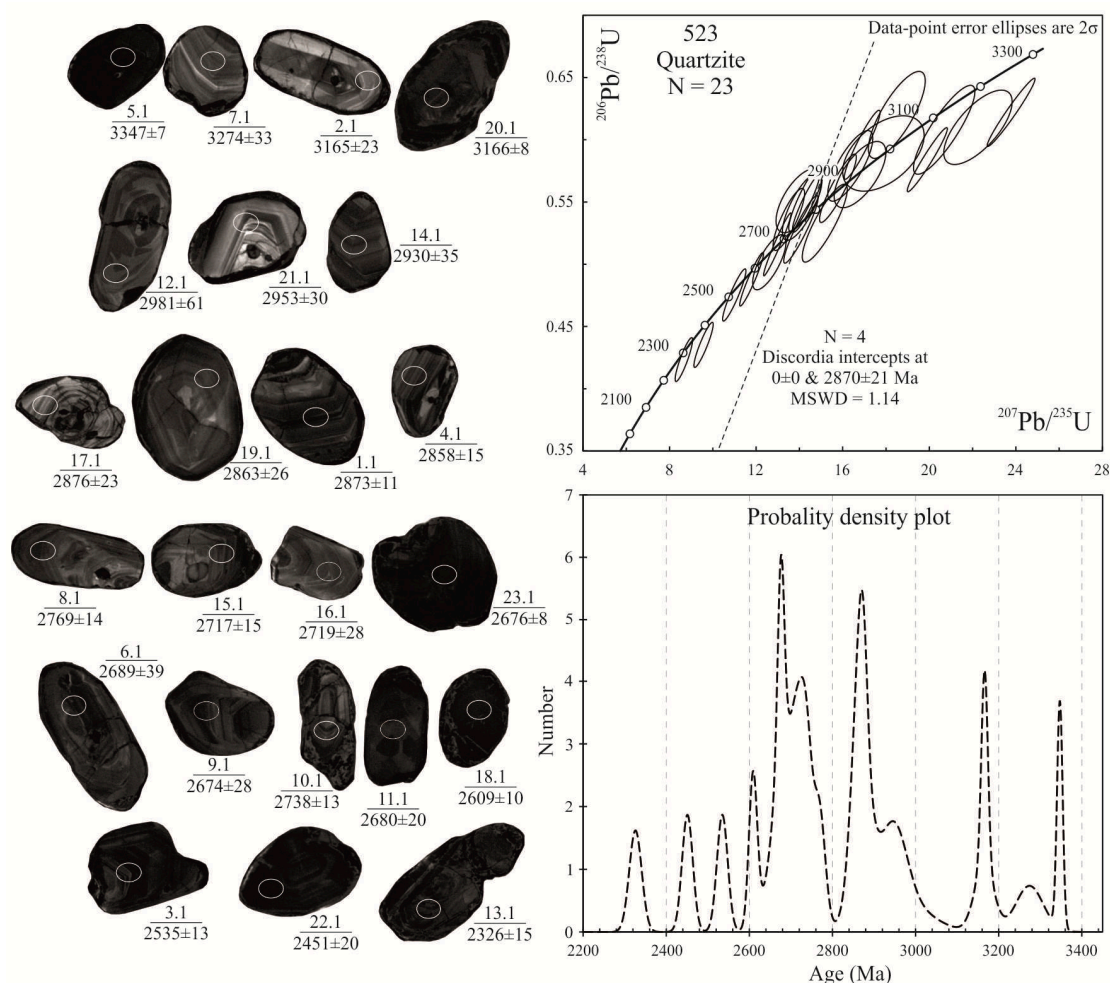
Figure 9. CL images and age of zircons from the quartzite, sample 523.

Twenty-three cores of zircon grains from the quartzite of sample 523 were dated (Figure 9). Four discordant Paleoarchean analyses (points with analyses 2.1, 5.1, 7.1, and 20.1) dated at 3347 ± 7 to 3166 ± 8 Ma (D = 3–7%) in the upper part of Figure 9 are the oldest. Two of the oldest grains display well-preserved rhythmic zoning (grains with points 2.1 and 7.1), show REE spectra (Figure 10a) most similar to magmatic type pattern [29] (ΣREE = 441–666 ppm), and are characterized by the lowest value of T_{Ti}^{Zir} = 768–784 °C in comparison with other analyses. The two other oldest grains (5.1, 20.1) are black in CL and are more enriched in Y 2277–3214 and REE (ΣREE = 1588–2136 ppm) due to an increase in HREE (ΣHREE = 1555–2096 ppm) and other factors (P, Th, Table S4).

Rhythmic zoning in a population of six grains dated at 2981–2858 Ma with analytical points 17.1 and 21.1 is similar to the magmatic pattern. Other grains display a spotted luminescence in CL, but they also lie in the magmatic zircons field in the REE distribution diagram (Figure 10b). The discordia line, based on four analyses from this population, shows an upper intersection at 2870 ± 21 Ma (MSWD = 1.14).

In a group of zircons dated 2769–2609 Ma (Figure 9), seven analyses yielded a mean age of 2695 ± 25 Ma (MSWD = 3.4). Rhythmic zoning in grains with analyses 8.1, 9.1, 15.1, and 16.1 was observed. Grains that are black in CL contain elevated LREE concentrations and display a decline in Eu-minimum (points 6.1, 18.1 23.1), suggesting zircon growth under fluid saturation conditions, and the maximum value of T_{Ti}^{Zir} = 817–858 °C is noted. As the age decreases from 2680 Ma, the Y (1231–1407 ppm) and HREE (826–1016 ppm) concentration increases respectively (Table S4). Magmatic zircons in the REE distribution diagram predominate (Figure 10c).
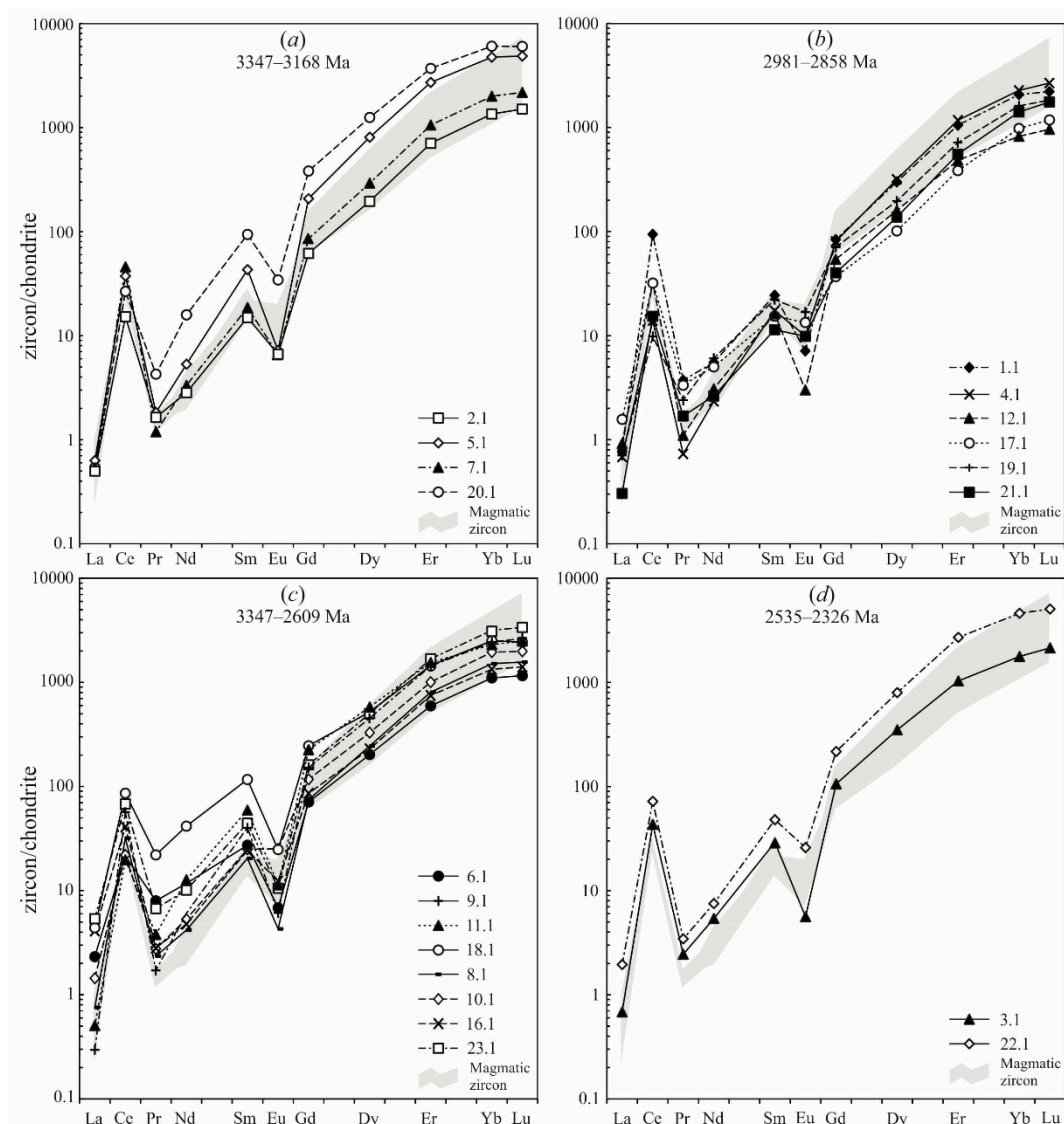
Figure 10. (**a**–**d**)—Chondrite-normalized REE patterns of zircons from the quartzite, sample 523. Pattern numbers correspond to the numbers of analytical spots in Figure 9. The grey field corresponds to the composition of magmatic zircons according to [29].

Zircons with a minimum age of 2535–2326 Ma yield a poor luminescence (Figure 9). Rhythmic zoning is only discernible in a grain with analysis 3.1 (dated at 2535 ± 13 Ma). The REE distribution spectra (Figure 10d) are most similar to the magmatic type. The zircons with analysis 22.1 (2451 Ma) have elevated Y, U, and REE concentrations and exhibit a decrease in Eu-minimum.

7. Sm-Nd Isotope Systematics

The Sm-Nd isotope system of rocks is considered in comparison with other granulites of the Kilegir and Bekelekh sequences of the Daldyn Group (Figure 11). The Sm-Nd isotope system in quartzites commonly indicates a low $^{147}Sm/^{144}Nd$ ratio of 0.0724–0.1111 (Table S5). However, the rocks in samples 823 and 823-1 show high $^{147}Sm/^{144}Nd$ ratio values of 0.1815–0.2541, exceeding the $^{147}Sm/^{144}Nd$ in chondrite. This makes it impossible to determine the Nd-model age of protolith and, as a consequence, the age of the rocks in the denudation area. All the rocks display negative $\varepsilon_{Nd}(T)$ values of −4.2 to −11.3 (Table S5). Considerable differences in the Nd-model age of the rock protolith are observed in two cases (samples 820 and 831-1) when the $T_{Nd}(DM\text{-}2st)$ = 3.69–3.71 Ga, and also for the quartzites of sample 523, where the $T_{Nd}(DM\text{-}2st)$ = 3.02 Ga.
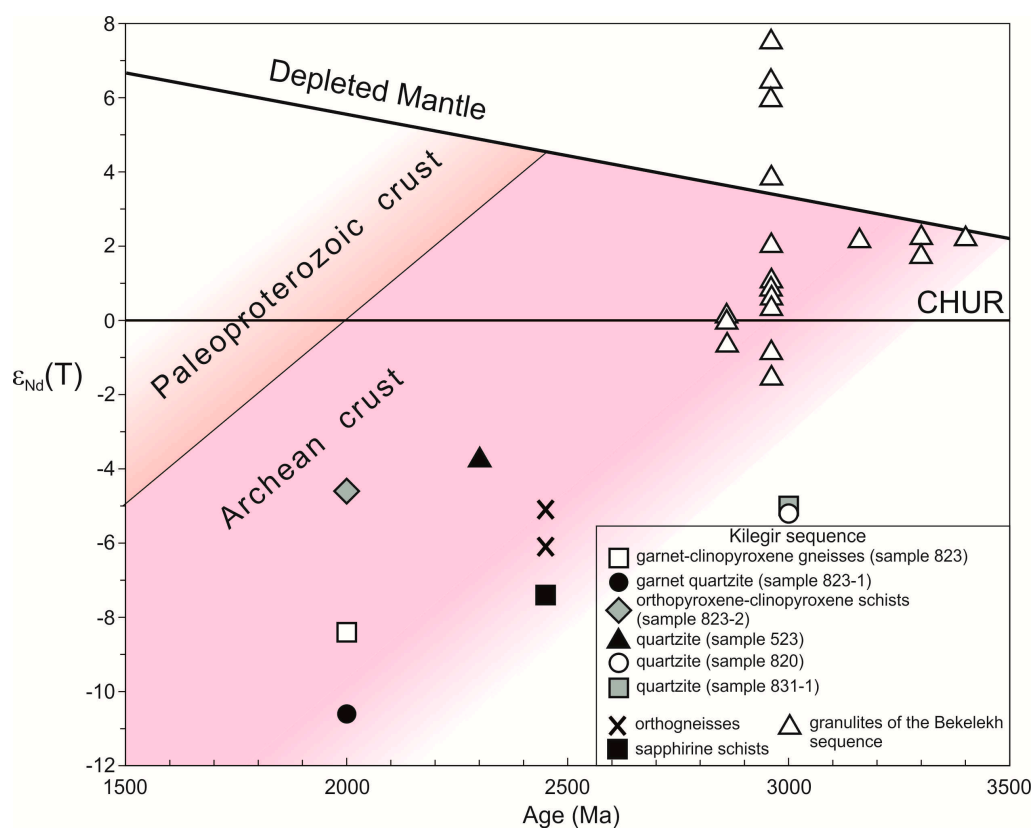
Figure 11. εNd versus age diagram for granulites of the Daldyn Group. Additionally, orthogneisses and sapphirine schists of the Kilegir sequence [30] and granulites of the Bekelekh sequence of the Daldyn Group are shown [7].

Sapphirine schists and orthogneisses of the Kilegir sequence [30], like the quartzites we studied, were characterized by negative values of $\varepsilon_{Nd}(T)$ from −7.4 to −5.1 and a model age of protolith $T_{Nd}(DM\text{-}2st)$ = 3.43–3.25 Ga. Thus, the protolith of the granulites of the Kilegir sequence studied by us and [30] was formed due to the processing of the Archean and Eoarchean continental crust.

Granulites of the Bekelekh sequence are represented by the prevailing clinopyroxene-orthopyroxene gneisses, containing interlayers of mafic and ultramafic schists. The age of the magmatic zircons varies from 3.40 to 2.86 Ga. The granulites have a magmatic protolith and are characterized by slightly negative and predominant positive $\varepsilon_{Nd}(T)$ values from −1.5 to +7.5 [7]. The protolith of granulites of the Bekelekh sequence indicates the formation of a juvenile Archean and Eoarchean crust with the participation of a depleted mantle source.

8. Discussion

Quartzite beds in the Daldyn Group occur in association with the two-pyroxene plagiogneisses, which are consistent in chemical composition with andesite or quartz diorite, with a U-Pb zircon age of 2960 ± 22 Ma [7]. The quartzites vary in the Nd-model age of the protolith and the age of detrital zircon. Quartzites in samples 820 and 831-1 with the model age of the protolith $T_{Nd}(DM\text{-}2St)$ = 3.69–3.71 Ga are dominated by Paleoarchean detrital zircons dated at 3.5 Ga [15], indicating the age of predominant magmatic rocks in the feeding province. The zircons in these quartzites, dated at 2778 ± 16 Ma, are metamorphic [15]. It is not clear whether this zircon formed prior to or after deposition in the sediment during Archean granulite-facies metamorphism. Therefore, the lower age boundary for the deposition of the sedimentary protolith of the quartzites is unknown.

In the quartzite of sample 523, whose model age of the protolith $T_{Nd}(DM\text{-}2St)$ is 3.02 Ga, the age of detrital zircon grains varies from Paleoarchean (3347 ± 7 Ma) to Paleoproterozoic (2451–2326 Ma).

No zircons with an age of 3.5 Ga have been revealed. The most numerous analyses of zircon grains show age peaks of 2870 ± 21 Ma (N = 6) and 2695 ± 25 Ma (N = 7), and are confined within the epochs of large-scale magmatism and metamorphism. For example, 2870 Ma detrital zircons were produced by the scour of the rocks formed by granulite-facies metamorphism and enderbitization (in sense of [31]) provoked by magmatism caused by the accretion of juvenile crust on the Anabar Shield and the reworking of the earlier crust in the age range 2878 ± 11–2858 ± 9 Ma [6,7]. The second peak of detrital zircons dated at 2695 ± 25 Ma is more likely to be associated with a new stage during the formation of juvenile crust, which is indicated by ultramafic intrusions dated at 2726 ± 15 Ma and potassium granitoid magmatism (2705 ± 12 charnockites [6], sanukitoids 2702 ± 9 [32], and the formation of anatectic alaskitic granite-gneiss dated at 2618 ± 10 Ma [7].

The 2535–2326 Ma zircons occur as scarce grains. Intrusions and metamorphic rocks of this age have not been established on the Anabar Shield.

Detrital zircon cores in sample 823-1 are 2758–2566 Ma old. Only zircons dated at 2758 ± 11 Ma are reliably identified as magmatic by rhythmic zoning and trace element concentrations.

In the quartzite (sample 831-1), zircons dated at 2778 ± 16 Ma are metamorphic and seem to have been produced by the same event as magmatic zircons dated at 2758 ± 11 Ma. It is this event that was identified as 2.75 Ga granulite-facies metamorphism at early stages in the study of the Anabar Shield [4].

Zircons, which are grey in CL, overgrow black cores in CL and form independent grains. These zircons yields a concordant age of 2000 ± 9 Ma, suggesting that the protolith of the quartzites cannot be younger than 2 Ga.

The trace element composition of zircon of 2000 ± 9 Ma is consistent with a magmatic type but displays a low Lu/Gd_N ratio of 2.6–9.2. These zircons were produced by partial rock melting under garnet stability conditions, i.e., granulite-facies metamorphism. Our findings confirm the results of studies presented by Peck et al. [33], which showed that the zircon growth in quartzites among granulites takes place in melt, and their U-Pb age shows the age of rock anatexis. However, the anomalous REE distribution spectra with negative LREE-anomalies on Figure 4 in quartzites and garnet-clinopyroxene gneisses (sample 823) suggest a metasomatic process similar to silicification with the removal of LREE [14]. Furthermore, in contrast to Peck et al. [33], the amount of overgrowth and the quantity of newly formed zircons is greater in SiO_2-enriched quartzites than in clinopyroxene gneisses, although the reverse pattern was expected [33]. It seems that rock anatexis in sample 823 at the postmagmatic stage was followed by silicification with the removal of LREE.

It should be noted that, although the Archean model age of the protolith $T_{Nd}(DM-2St)$ is 3.25–3.43 Ga, the scarce age values for the cores of detrital zircon in sapphirine-bearing schist from the Kilegir sequence of the Anabar Shield yield a Paleoproterozoic age and show an age of 2217 ± 6 Ma (D = 1%) in the least discordant zircon [30].

Thus, the sedimentation time for the sedimentary protolith of the para-rocks in the Daldyn Group is between the age of the youngest detrital zircons, 2250 ± 24 Ma (2217 ± 6 Ma, as dated by [30]), and the time of quartzite anatexis under the granulite-facies conditions of metamorphism (2000 ± 9 Ma). The time of formation for the sedimentary protolith of quartzites and paragneisses could tentatively be accepted as 2.1 Ga.

It is not yet clear whether other quartzite bodies (Figure 3) in which no Paleoproterozoic detrital zircons were revealed are Proterozoic; however this possibility is not ruled out [15]. The occurrence of Paleoproterozoic metasedimentary rocks in the Daldyn Group suggests that the Daldyn granulite group, as it looks like now, is tectonically heterogeneous and contains Paleoproterozoic rock bodies among predominant Archean rocks. A similar situation has been described from the well-studied Jack Hills sedimentary belt in Australia, where ~3 Ga conglomerates host the Earth's oldest zircons. It gradually became obvious that rocks with Proterozoic zircons make up 12% of the belt, suggesting the tectonic alternation of Archean and Proterozoic rock sequences [12].

9. Conclusions

Quartzites occurring at the boundary between the Bekelekh and Kilegir sequences in the Daldyn Group differ markedly in the Nd-model age of the protolith and the U-Pb age of detrital zircons. One group of rocks with the Nd-model age of the protolith with a T_{Nd}(DM-2St) of 3.69–3.71 Ga contains predominant detrital zircons dated at 3487 ± 21 Ma. Another group with a T_{Nd}(DM-2St) of 3.02 Ga hosts Paleoproterozoic zircons. Furthermore, Paleoproterozoic detrital zircons were revealed in paragneisses and quartzites with a disturbed isotope system, whose model age is not clear. These rocks have been altered metasomatically, and the zircon neoformation in them is well-defined. Newly formed zircons display geochemistry of magmatic type in spite of zoning typical of granulite zircons.

The age of the youngest detrital zircons is 2250 ± 24 Ma and the age of the anatectic rims is 2000 ± 9 Ma. The formation time for the sedimentary protolith of gneisses and quartzites lies within the interval between the two age values specified above and is provisionally taken as 2.1 Ga. The presence of Paleoproterozoic metasedimentary rocks in the Daldyn Group has led us to conclude that the Daldyn granulite group, as it now looks, is tectonically heterogeneous and contains Paleoproterozoic rock bodies among predominant Archean rock sequences.

References

1. Rosen, O.M.; Condie, K.C.; Natapov, L.M.; Nozhkin, A.D. Archean and early Proterozoic evolution of the Siberian Craton: A preliminary assessment. *Archean Crustal Evol.* **1994**, *11*, 411–459.
2. Gladkochub, D.; Pisarevsky, S.; Donskaya, T.; Natapov, L.; Mazukabzov, A.; Stanevich, A.; Sklyarov, E. The Siberian Craton and its evolution in terms of the Rodinia hypothesis. *Episodes* **2006**, *29*, 169–174. [CrossRef]
3. Shatsky, V.S.; Malkovets, V.G.; Belousova, E.A.; Tretiakova, I.G.; Griffin, W.L.; Wang, Q.; Ragozin, A.L.; Gibsher, A.A.; O'Reilly, S.Y. Multi-stage modification of Paleoarchean crust beneath the Anabar tectonic province (Siberian craton). *Precambr. Res.* **2018**, *305*, 125–144. [CrossRef]
4. Bibikova, E.V. *U-Pb Geochronology of Early Stages of Development of Ancient Shields*; Nauka: Moscow, Russia, 1989; p. 179. (In Russian)
5. Gusev, N.I.; Rudenko, V.E.; Berezhnaya, N.G.; Skublov, S.G.; Larionov, A.N. Isotope-geochemical features and age (SHRIMP II) of metamorphic and igneous rocks in the Kotuykan-Monkholinsky zone of the Anabar shield. *Reg. Geol. Metallog.* **2013**, *54*, 45–59. (In Russian)
6. Gusev, N.I.; Rudenko, V.E.; Sergeeva, L.Yu.; Lokhov, K.I.; Berezhnaya, N.G.; Larionov, A.N. Archean granulites of Dzhelinda blok Anabar Shield (Siberian Craton): Geochemistry, age, isotopic characteristics. *Reg. Geol. Metallog.* **2016**, *66*, 30–44. (In Russian)

7. Gusev, N.I.; Sergeeva, L.Y.; Skublov, S.G.; Berezhnaya, N.G.; Larionov, A.N. Composition and relations of Early and Late Archean granulites in the Bekelekhskaya sequence of the Anabar Shield (Siberian Craton). *Reg. Geol. Metallog.* **2017**, *70*, 17–35. (In Russian)

8. Gusev, N.I.; Sergeeva, L.Y.; Skublov, S.G. Evidence of the reworked Eoarchean crust in the Anabar Shield (Siberian Craton). *Reg. Geol. Metallog.* **2019**, *78*, 40–57. (In Russian)

9. Bibikova, E.V.; Fedotova, A.A.; Claesson, S.; Stepanyuk, L.M. Early crust of the Podolia Domain of the Ukrainian Shield: Isotopic age of terrigenous zircons from quartzites of the Bug Group. *Strat. Geol. Correl.* **2015**, *23*, 555–567. [CrossRef]

10. Bolhar, R.; Hofmann, A.; Kemp, A.I.S.; Whitehouse, M.J.; Wind, S.; Kamber, B.S. Juvenile crust formation in the Zimbabwe Craton deduced from the O-Hf isotopic record of 3.8-3.1 Ga detrital zircons. *Geochim. Cosmochim. Acta* **2017**, *215*, 432–446. [CrossRef]

11. Kielman, R.B.; Nemchin, A.A.; Whitehouse, M.J.; Pidgeon, R.T.; Bellucci, J.J. U-Pb age distribution recorded in zircons from Archean quartzites in the Mt. Alfred area, Yilgarn Craton, Western Australia. *Precambr. Res.* **2018**, *310*, 278–290. [CrossRef]

12. Wang, Q.; Wilde, S.A. New constraints on the hadean to Proterozoic history of the Jack Hills belt, Western Australia. *Gondwana Res.* **2018**, *55*, 74–91. [CrossRef]

13. Zimmermann, U.; Andersen, T.; Madland, M.V.; Larsen, I.S. The role of U-Pb ages of detrital zircons in sedimentology—An alarming case study for the impact of sampling for provenance interpretation. *Sediment. Geol.* **2015**, *320*, 38–50. [CrossRef]

14. Sazonov, V.N.; Vikent'eva, O.V.; Ogorodnikov, V.N.; Polenov, Y.A.; Velikanov, A.Y. Rare-earth elements in columns of propilitization, albititization, eisitization, berezitization-listvenitization of differentsialic rocks: Evolution of distribution, causes and practical importance. *Litosfera* **2006**, *3*, 108–124. (In Russian)

15. Sergeeva, L.Y.; Gusev, N.I.; Skublov, S.G. U-Pb age and geochemistry of detrital zircon from quartzites of the Daldyn Group (Anabar Shield). *Geochem. Int.* **2020**, *6*, 609–617.

16. Williams, I.S. U-Th-Pb geochronology by ion-microprobe. *Rev. Econ. Geol.* **1998**, *7*, 1–35.

17. Ludwig, K.R. *SQUID 1.00. A User's Manual*; Berkeley Geochronology Center Special Publication: Berkeley, CA, USA, 2000; Volume 2.

18. Black, L.P.; Kamo, S.L.; Allen, C.M.; Aleinikoff, J.N.; Davis, D.W.; Korsch, R.J.; Foundoulis, C. TEMORA 1: A new zircon standard for Phanerozoic U-Pb geochronology. *Chem. Geol.* **2003**, *200*, 155–170. [CrossRef]

19. Ludwig, K.R. *User's Manual for Isoplot/Ex. Version 2.10*; A geochronological toolkit for Microsoft Excel; Berkeley Geochronology Center Special Publication: Berkeley, CA, USA, 1999; Volume 1.

20. Fedotova, A.A.; Bibikova, E.V.; Simakin, S.G. Ion-microprobe zircon geochemistry as an indicator of mineral genesis during geochronological studies. *Geochem. Int.* **2008**, *9*, 980–997. [CrossRef]

21. Watson, E.B.; Wark, D.A.; Thomas, J.B. Crystallization thermometers for zircon and rurile. *Contrib. Mineral. Petrol.* **2006**, *151*, 413–433. [CrossRef]

22. Jacobsen, S.B.; Wasserburg, G.J. Sm-Nd evolution of chondrites and achondrites. *Earth Planet. Sci. Lett.* **1984**, *67*, 137–150. [CrossRef]

23. Goldstein, S.J.; Jacobsen, S.B. Nd and Sm isotopic systematics of river water suspended material: Implications for crustal evolution. *Earth Planet. Sci. Lett.* **1988**, *87*, 249–265. [CrossRef]

24. Whitney, D.L.; Evans, B.W. Abbreviations for Names of Rock-Forming Minerals. *Am. Mineral.* **2010**, *95*, 185–187. [CrossRef]

25. Werner, C.D. Saxonian granulites—Igneous or lithogenous: A contribution to the geochemical diagnosis of the original rocks in hig-metamorphic complexes. *Gerlands Beitr. Geophys.* **1987**, *96*, 271–290.

26. Sun, S.; McDonough, W.F. Chemical and isotopic systematics of oceanic basalts: Implications for mantle composition and processes. *Geol. Soc. Spec. Publ.* **1989**, *42*, 313–345. [CrossRef]

27. Rollinson, H.R. *Using Geochemical Data: Evolution, Presentation, Interpretation*; Longman scientific and technical: London, UK, 1993; p. 352.

28. Corfu, F.; Hanchar, J.M.; Hoskin, P.W.O.; Kinny, P. Atlas of zircon textures. *Rev. Mineral. Geochem.* **2003**, *53*, 469–500. [CrossRef]

29. Hoskin, P.W.O. Trace-element composition of hydrothermal zircon and the alteration of Hadean zircon from the Jack Hills, Australia. *Geochim. Cosmochim. Acta* **2005**, *69*, 637–648. [CrossRef]

30. Nozhkin, A.D.; Likhanov, I.I.; Krylov, A.A.; Savko, K.A.; Serov, P.A. Sapphirine-bearing granulites of the Anabar Shield. *Geochem. Int.* **2019**, *57*, 524–539. [CrossRef]

31. Korikovsky, S.P.; Aranovich, L.Y. Charnockitization and enderbitization of mafic granulites in the Porya Bay area, Lapland Granulite Belt, Southern Kola Peninsula: I. Petrology and geothermobarometry. *Petrology* **2010**, *18*, 320–349. [CrossRef]

32. Gusev, N.I.; Rudenko, V.E.; Berezhnaya, N.G.; Skublov, S.G.; Moreva, N.V.; Larionov, A.N.; Lepehina, E.N. Age of granulites of Daldyn series of Anabar Shield. *Reg. Geol. Metallog.* **2012**, *52*, 29–38. (In Russian)

33. Peck, W.H.; Bickford, M.E.; Mclelland, J.M.; Nagle, A.N.; Swarr, G.J. Mechanism of metamorphic zircon growth in a granulite-facies quartzite, Adirondack Highlands, Grenville Province, New York. *Am. Mineral.* **2010**, *95*, 1796–1806. [CrossRef]